https://doi.org/10.1016/j.vacuum.2020.109952

Monte Carlo simulation of polydisperse particle deposition and coagulation dynamics in enclosed chambers

Hongmei Liu[1,2], Wei Jiang[1], Wenming Liu[1], Xuedong Liu[1,2], Shuyuan Liu[3,*], Tat Leung Chan[4]

1. School of Mechanical Engineering and Rail Transit, Changzhou University, Changzhou, 213164, China

2. Jiangsu Key Laboratory of Green Process Equipment, Changzhou 213164, China

3. Science and Technology on Combustion, Internal Flow and Thermal-Structure Laboratory, Northwestern Polytechnical University, Xi'an, 710072, China

4. Department of Mechanical Engineering, The Hong Kong Polytechnic University, Kowloon, Hong Kong

*Corresponding author. E-mail address: liushuyuan@nwpn.edu.cn (S. Liu)

Abstract

A novel Monte Carlo method is proposed to improve the computational accuracy and efficiency of Monte Carlo methods in examining the polydisperse micro- and nano-particle dynamics including deposition and coagulation processes in enclosed or vacuum chambers. In the original differentially weighted Monte Carlo (DWMC) method, the coagulation and deposition events are both treated by stochastic approaches. In the present study, the deposition event is solved by a deterministic method where a proportion of the deposited real particles inside a simulated particle is determined by a probability related to the deposition kernel. Furthermore, the operator splitting method is adopted to couple the stochastic and deterministic processes. This method is verified against both analytical solutions and experimental results for particle deposition and coagulation dynamics. The particle size distributions are obtained and the results exhibit excellent accordance with the corresponding analytical solutions and experimental results. Compared with the original DWMC method, the simulation results show that the proposed Monte Carlo

method can obtain very favorable improvement in both computational accuracy and efficiency.

Keywords: Monte Carlo simulation, particle size distribution, deposition, coagulation, sodium chloride aerosols, paper ash particles

1. Introduction

Particle dynamics including deposition and coagulation processes are quite common in both engineering applications and natural phenomena, such as the precipitation of rain, snow and fog [1]; the removal process of fly ash particles in thermal power plant [2]; the migration process of smoke particles from exhaust pipe of the vehicle [3]; chemical vapor deposition and micro- or nano-particle synthesis in pharmaceutical and chemical industry [4,5], etc. In these areas, the particle deposition and coagulation processes are quite crucial in determining the particle size distributions which will affect the physical and chemical properties, such as, the toxicity, radioactivity, light scattering and so on [6,7]. Furthermore, the highly concentrated indoor micro- and nano-particles could cause great concerns about both environmental damage and human health and have attracted people's attentions nowadays [8]. Thus, the dynamical behaviors including deposition and coagulation of the particles are of vital importance in the study of indoor ultrafine particles. Therefore, the understanding of the variation of particle size distributions resulting from deposition and coagulation processes appears to be particularly important.

The micro- and nano-particles are either released directly into the atmosphere or produced by natural or human behaviors. In the formation and growth process, the particles undergo several chemical and physical transformations. In the first step of particle formation process, a critical size of nucleus is formed

from vapor and then the nucleus grows up gradually to form a larger size particle, during which a critical free energy is required to obtain stable particles with critical radius [9]. The nucleation process results in a decrease in both enthalpy and entropy. A free-energy barrier needs to be overcome before the phase transition becomes spontaneous [10,11]. In the following particle growth process, particle will experience dynamical processes, such as, collision, coagulation, deposition and so on. And for a specific system with only coagulation and deposition, the thermodynamic theory also works in a qualitative understanding that stochastic processes increase the entropy and reduce Gibbs free energy.

The particle dynamical mechanisms can be quite complicated in different applications. For example the deposition mechanisms include Brownian diffusion, gravitational sedimentation, turbulent impaction, interception and inertial impaction, wet removal and so on [1,12]; the coagulation mechanisms include Brownian diffusion, turbulent diffusion, thermal motion, electrical charges, preferential concentration and so on [13]. In different regimes, the mechanisms and importance of deposition and coagulation will be different. Okuyama et al. [14] investigated the aerosol dynamical behaviors experiencing Brownian coagulation, Brownian diffusive deposition and gravitational sedimentation numerically and experimentally and studied the controlling domain of these three factors. Hussein et al. [15] and Rim et al. [16] estimated the deposition rates of ultrafine particle size distributions considering the coagulation effect and concluded that coagulation becomes significant for ultrafine particles when the total number concentration is higher than 10^4 cm^{-3}. Yu et al. [17] investigated the evolution of ratio of coagulation to deposition in a ventilated chamber and found that the variation heavily depends on the particle size

distributions and vary in different regimes. Xiao et al. [18] investigated the deposition rate and coagulation coefficients of indoor particles and found that the deposition and coagulation rates both increase with the increase of air temperature and the enhancement of indoor air mixing intensity.

Since it is quite difficult to derive the analytical solutions or to do experiments for describing particle dynamics considering such complicated factors, numerical simulation methods tend to be quite popular in predicting particle dynamical processes [19]. In the previously proposed numerical methods, the most widely used methods are the method of moment (MOM) [17–21], sectional method (SM) [25,26], and Monte Carlo (MC) method [1,27,28]. Both of the MOM and SM are deterministic methods [29,30], which are relatively accurate and efficient for describing the particle size distributions in single-component and monodispersed particle systems. Nevertheless, it is quite complicated or difficult to predict the particle size distributions in multicomponent and polydisperse particle systems using these two methods.

Monte Carlo (MC) methods have become more and more preferred by researchers recently due to its advantages in describing the multicomponent and polydisperse particle systems. MC methods imitate the particle dynamical behaviors with a cluster of fictitious or simulated particles, thus the specific information of the particles can be included in the algorithm and it is also easy to obtain the history, trajectory and structural information of the particles using MC method [31]. However, one disadvantage of MC method is its high requirement of computational cost. Weighted Monte Carlo methods [32–34] were proposed to obtain higher precision and efficiency of MC methods. Herein, the further development and improvement of the differentially weighted operator splitting Monte Carlo (DWOSMC) method is presented for

describing polydisperse particle deposition and coagulation dynamics in enclosed chambers which is based on the differentially weighted Monte Carlo (DWMC) algorithm proposed by Zhao et al. [1,35,36].The DWOSMC method is proven capable of predicting the evolution of particle number concentrations, particle geometric mean size and particle size distributions (PSDs) considering particle deposition and coagulation dynamics. The results are validated through both analytical solutions and experimental results.

2. Methods

2.1 Thermodynamic theory and dynamical equations

2.1.1 Thermodynamic theory

Thermodynamics studies equilibrium based on the second law of thermodynamics: in an isolated system, entropy increases in all spontaneous processes. In a thermodynamic process, the Gibbs free energy change is, $\Delta G=\Delta H-T\Delta S$ (where ΔH is the enthalpy change and ΔS is the entropy change). If $\Delta G<0$, the thermodynamic process would happen spontaneously, which also works for the formation and growth of particles [10,37]. In the nucleation process of particles, the competition between the enthalpy release and the entropy decrease determines the energy barrier for nucleus formation and the Gibbs free energy change determines the critical cluster size [9–11]. Thus, the formation or the driving force of particle nucleation process could be explained by a thermodynamic process or the Gibbs free energy change. And for a specific particle system with only coagulation and deposition, the thermodynamic theory is implicitly included in the model formulation of coagulation and deposition kernels considering the stochastic processes that occur

in the system studied. The physical principles also work in a qualitative understanding that stochastic processes increase the entropy and reduce Gibbs free energy.

2.1.2 Dynamical equations

The variation of PSD considering deposition and coagulation processes is expressed by the general dynamic equation (GDE) [38],

$$\frac{\partial n(\upsilon,t)}{\partial t}=\left[\frac{\partial n(\upsilon,t)}{\partial t}\right]_{\text{coag}}+\left[\frac{\partial n(\upsilon,t)}{\partial t}\right]_{\text{depo}} \tag{1}$$

where υ is the size of particles, υ may refer to the volume, radius or the diameter, n is the particle number density with a size υ. Eq. (1) represents the variation of the number density of particles with size υ due to coagulation which is described in Eq. (6) and change of number density attributable to deposition processes which is described in Eq. (9), respectively.

Coagulation refers to the process that two particles collide and stick together. Assuming N_{ij} is the collision frequency between two spherical particles i and j per unit volume per unit time, then the collision frequency is [19],

$$N_{ij}=\beta_{ij}n_i n_j \tag{2}$$

where β_{ij} is the particle collision frequency function.

In case of coagulation, the rate of formation of particles with size υ_k is

$$n_{\text{form}}=\frac{1}{2}\sum_{\upsilon_k=\upsilon_i+\upsilon_j}N_{ij} \tag{3}$$

where $\upsilon_k=\upsilon_i+\upsilon_j$, and the factor of ½ is introduced because each collision is counted twice in the summation. the rate of loss of particles with size υ_k is,

$$n_{\text{loss}} = \sum_{i=1}^{\infty} N_{ik} \tag{4}$$

Therefore, the net rate of generation of particles with size υ_k is [19],

$$\frac{dn_k}{dt} = n_{\text{form}} - n_{\text{loss}} = \frac{1}{2} \sum_{\upsilon_k = \upsilon_i + \upsilon_j} N_{ij} - \sum_{i=1}^{\infty} N_{ik} \tag{5}$$

which can be further expressed as Eq. (6).

$$\left[\frac{\partial n(\upsilon, t)}{\partial t} \right]_{\text{coag}} = \frac{1}{2} \int_0^{\upsilon} \beta(\upsilon', \upsilon - \upsilon') n(\upsilon, t) n(\upsilon - \upsilon', t) \mathrm{d}\upsilon - n(\upsilon, t) \int_0^{\infty} \beta(\upsilon, \upsilon') n(\upsilon', t) \mathrm{d}\upsilon' \tag{6}$$

where $\beta(\upsilon, \upsilon')$ is the particle coagulation kernel between particles with size υ and particles with size υ'.

There are different expressions for the coagulation kernel with varying size regime. In the free molecular regime, the coagulation kernel is expressed as [19],

$$\beta_{ij} = (3/4\pi)^{1/6} (6k_b T/\rho)^{1/2} \left(\frac{1}{v_i} + \frac{1}{v_j} \right)^{1/2} \left(v_i^{1/3} + v_j^{1/3} \right)^2 \tag{7}$$

In the continuum regime, the coagulation kernel is expressed as [19],

$$\beta_{ij} = \frac{2k_b T}{3\mu} \left(v_i^{1/3} + v_j^{1/3} \right) \left(\frac{1}{v_i^{1/3}} + \frac{1}{v_j^{1/3}} \right) \tag{8}$$

The change of number density attributable to deposition processes is described as follows.

$$\left[\frac{\partial n(\upsilon, t)}{\partial t} \right]_{\text{depo}} = -R(\upsilon) n(\upsilon, t) \tag{9}$$

$R(\upsilon)$ is the deposition rate which could result from Brownian diffusion, gravitational sedimentation, electrical and thermal forces.

2.2 DWOSMC method for simulating deposition and coagulation dynamics

2.2.1 The choice of time-step

The characteristic timescale of coagulation process is the following [36,39] .

$$\tau_{\mathrm{coag}} = \min|_{\forall i}\left(V_{\mathrm{s}} / \sum_{j=1, j\neq i}^{N_{\mathrm{s}}} \beta_{ij}^{'}\right) \tag{10}$$

where N_{s} and V_{s} are the number of simulated particles, and the volume of computational simulation system (the volume of the chamber in the present study), respectively. $\beta_{\mathrm{ij}}^{'}$ is the normalized coagulation kernel of simulated particles i and j taking the factors of "weight" into consideration, which is as follows.

$$\beta_{ij}^{'} = 2\beta_{ij} w_j \max(w_i, w_j) / (w_i + w_j) \tag{11}$$

For deposition processes, the characteristic timescale is expressed as:

$$\tau_{\mathrm{depo}} = \min|_{\forall i}\left(1 / R_i\right) \tag{12}$$

where R_i is the deposition kernel.

A suitable time-step, τ should be used which is smaller than both the characteristic timescales of deposition and coagulation processes. Therefore, an empirical parameter, α is utilized herein, and τ is described as:

$$\tau = \alpha \times \min\left(\tau_{\mathrm{coag}}, \tau_{\mathrm{depo}}\right) \tag{13}$$

The empirical parameter, α is a multiplicative factor and is usually set as 0.01 or less to ensure that the particle dynamical events are uncoupled within a time step [32,34,40]. In the present study, α has a value of 0.001-0.01.

2.2.2 The treatment of coagulation events

The treatment of coagulation events is referring to the differentially weighted Monte Carlo (DWMC) method and is described as follows [35,39].

The DWMC method tracks each simulated particle to check whether coagulation takes place on

particle *i* based on the following equation.

$$P_{\text{coag},i} = 1 - \exp(-V_s C_i \tau / 2) \tag{14}$$

$$C_i = \frac{1}{V_s^2} \sum_{j=1, j\neq i}^{N_s} \beta_{ij}^{'} \tag{15}$$

Afterwards, a random number r_1 is selected which is uniformly distributed between (0,1), if Eq. (16) is satisfied, particle *i* is regarded as the first partner participating in the coagulation event, otherwise, next simulation particle is tracked.

$$r_1 \leq P_{\text{coag},\, i} \tag{16}$$

The second coagulation partner is chosen using the acceptance-rejection method, if Eq. (17) is satisfied, particle *j* is selected as the second coagulation partner.

$$r_2 \leq \beta_{ij}^{'} / \max(\beta_{mn}^{'})\,|_{\forall m, \forall n} \tag{17}$$

where r_2 is another random number selected between (0,1) which is also uniformly distributed.

Once the coagulation pair *i* and *j* are determined, coagulation would be managed as Eq. (18) where the conservation of volume is considered.

$$\begin{aligned} &\text{If } w_i = w_j, \begin{cases} w_i^{'} = w_i / 2; v_i^{'} = v_i + v_j \\ w_j^{'} = w_i / 2; v_j^{'} = v_i + v_j \end{cases} \\ &\text{If } w_i \neq w_j, \begin{cases} w_i^{'} = \max(w_i, w_j) - \min(w_i, w_j); v_i^{'} = v_m\,|_{w_m = \max(w_i, w_j)} \\ w_j^{'} = \min(w_i, w_j); v_j^{'} = v_i + v_j \end{cases} \end{aligned} \tag{18}$$

where $w_{\text{i}}^{'}$, $w_{\text{j}}^{'}$, $v_{\text{i}}^{'}$ and $v_{\text{j}}^{'}$ denote the weight and volume of the produced numerical particles *i* and *j* after the treatment of coagulation process.

2.2.3 The treatment of deposition events

In the DWMC method, the calculation of deposition event on particle i is also based on the probabilistic process and stochastic approach: the probability of simulated particle i depositing is defined as $P_{\text{depo},i}$, if Eq. (19) is satisfied, then particle i will be scavenged and will no longer be tracked. Instead, a stochastic process will be employed to select a random simulated particle j : the index of particle j would be determined by Eq. (20). In this selection process, it should be confirmed that the particle index j is not the same with i. Once j is selected, it will be split into two new simulated particles i' and j' [1] to maintain constant number of the simulated particles. Afterwards, the deposition event would be managed as Eq. (21).

$$r_3 \le P_{\text{depo},i} \tag{19}$$

$$j = \text{integer}[r_4 \times N_s] \tag{20}$$

$$\begin{aligned} w_i' &= w_j' = w_j / 2 \\ v_i' &= v_j' = v_j / 2 \end{aligned} \tag{21}$$

In the present study, the treatment of deposition events is different from the DWMC method. The deposition event is solved by a deterministic method: if the probability of deposition taking place in simulated particle i is $P_{\text{depo},i}$, then it is assumed that the proportion of the deposited real particles inside simulated particle i is $P_{\text{depo},i}$. Therefore, after the deposition event, the weight of particle i, w_i, will be changed according to the following equation.

$$w_i' = w_i \times (1 - P_{\text{depo,i}}) \tag{22}$$

where the probability of particle i depositing within τ, $P_{\text{depo,i}}$, is expressed as Eq. (23) [41].

$$P_{\text{depo,i}} = 1 - \exp(-R_i \tau) \tag{23}$$

where R_i is the deposition kernel of particle i.

2.2.4 The flowchart of DWOSMC method

Herein, a differentially weighted operator splitting Monte Carlo (DWOSMC) method is further developed for predicting the evolution of PSDs considering deposition and coagulation in polydisperse particle systems. In this method, the deposition event is solved by a deterministic approach, and the coagulation event is solved by a stochastic method.

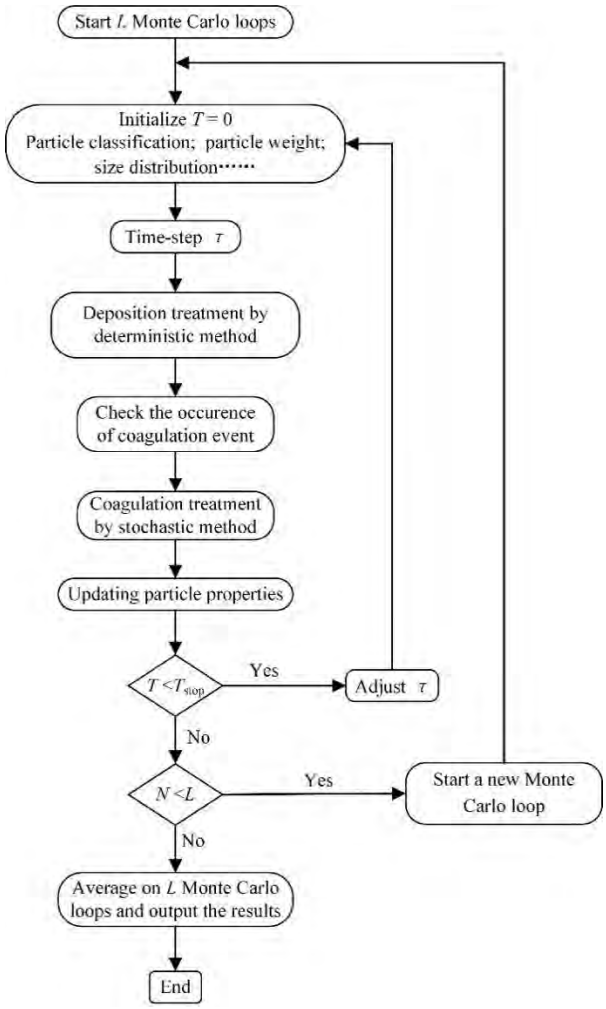

Fig. 1 Illustration of DWOSMC algorithm for simulating deposition and coagulation processes.

The flowchart of the DWOSMC method for describing deposition and coagulation processes is

described as follows:

(1) Start and predetermine the total MC loops, L.

(2) Initialize the particle system. The polydisperse particles are classified into several sections and the initial parameters of particle properties (size distribution, weight, etc.) is firstly assigned. The weights of simulated particle i, w_i is defined as,

$$w_i = \frac{N_{\text{real}}(\upsilon)}{N_{\text{simulated}}(\upsilon)} \tag{24}$$

(3) Determine a time-step τ according to Section 2.2.1.

(4) Particle dynamical processes integration. Particle deposition and coagulation processes are calculated by deterministic and stochastic methods, respectively, and then the calculated results are integrated by applying the operator splitting method as the following [42]:

$$\exp(\tau\psi) = \exp(\tau\psi\mathrm{d})\exp(\tau\psi\mathrm{s}) + o(\tau^2) \tag{25}$$

where Ψ represents the total particle dynamical processes, Ψ_{d} represents the deposition process, and Ψ_{s} represents the coagulation process.

Within τ, the deposition event is first calculated and then the coagulation event is treated.

(5) Handle the deposition process according to Section 2.2.3.

(6) Handle the coagulation process according to Section 2.2.2.

(7) The properties and parameters of the simulated particles (size distribution, weight, etc.) will be updated.

(8) Judgement of the status of the current MC loop: If the present simulation time, T reaches

the simulation end time T_s, exit the current MC loop. If not, repeat steps (3) to (7).

(9) Judgement of the status of the numerical simulation: If the present MC loop number N is smaller than L, start a new MC loop. If N equals to L, the mean value of the particle information should be calculated to output the properties of the particle system.

The flowchart of the DWOSMC model scheme for simulating deposition and coagulation processes is presented in Fig. 1.

3. Results and Discussion

In the present study, the capability of DWOSMC method is validated by seven cases considering different particle dynamic processes in different mechanisms in enclosed chambers. In the first two cases, deposition processes considering the mechanisms of gravitational effect and Brownian diffusion are considered where analytical solutions exist [43]; in Case C, aerosol particle precipitation by raindrops is investigated where analytical solutions exist [44]; in Case D and Case E, deposition and coagulation processes are considered where analytical solutions also exist [45]. For the sake of comparing the computational precision and efficiency, the results of DWMC method are also presented for the purpose of comparison in the first five cases. Afterwards, the DWOSMC method is validated against the experimental results in two cases where sodium chloride aerosol dynamics [46] and paper ash particle dynamics [47] are considered, respectively. Lastly, the DWOSMC method is used to study the particle dynamics in a vacuum chamber for the first time. Herein, unless otherwise stated, the number of simulated particles used is 3000, and the particles are split into 200 sections for the purpose of describing the particle size distributions.

3.1 Case A and Case B: deposition processes

In Cases A and B, the initial particles have a log-normal size distribution according to Eq. (26) [43].

$$n_{\mathrm{p}}(r,0)=\frac{1}{r}\frac{N_0}{\sqrt{2\pi}\ln\sigma_0}\exp\left(-\frac{\ln^2(r/r_{\mathrm{g0}})}{2\ln^2\sigma_0}\right) \tag{26}$$

where N_0, r_{g0}, σ_0 are the initial particle number density, initial geometric mean radius and the geometric standard deviation, respectively.

The initial conditions and numerical settings used for Cases A and B are summarized in Table 1.

Table 1 Initial conditions and numerical settings for Cases A and B.

Cases	N_0 ($\mathrm{m^{-3}}$)	r_{g0} (μm)	σ_0	R ($\mathrm{s^{-1}}$)	t_{stop} (s)
A	1×10^6	3	1.5	R_{g}	20000
B	1×10^6	0.1	1.5	$R_{\mathrm{g}}+R_{\mathrm{d}}$	1560

R_{g} is the deposition kernel in gravitational-dominant size range, and is expressed as the following equation.

$$R_{\mathrm{g}}(r,t)=Br^2 \tag{27}$$

where $B=2\rho g/9\mu H$, ρ=2000kg/m^3, g=9.782m/s^2, $\mu=3.14\times10^{-5}$kg/(m·s), H=2.5m.

R_{d} is deposition kernel in diffusion-dominant range, and is expressed as the following equation.

$$R_{\mathrm{d}}(r,t)=Ar^{-2(n-1)/n} \tag{28}$$

$$A=\left(\frac{1.7\lambda k_B T}{6\pi\mu}\right)^{(n-1)/n}\left(\frac{nS\sin(\pi/n)\sqrt[n]{k_e L_2^{2-n}}}{\pi V}\right) \tag{29}$$

$$L_2 = \frac{L}{\sqrt{\mathrm{Re}}} \tag{30}$$

where $\lambda=2\times10^{-8}$ m, $k_B=1.38054\times10^{-8}$ J·K, $k_e=36$ s^{-1}, $T=433.15$ K, $L=1$ m, Re=3000, V = 3m×5m×2.5m.

In Case A, the deposition process in gravitational-dominant size range is considered as is shown in Table 1. Since for relatively large particles, the gravitational deposition effect will dominate the particle size distribution evolution. The change of normalized particle number density and normalized particle geometric mean radius over time for is shown in Fig. 2, and the evolution of PSDs for several time periods (t = 0 s, 700 s, 2000 s, 5000 s) is shown in Fig. 3.

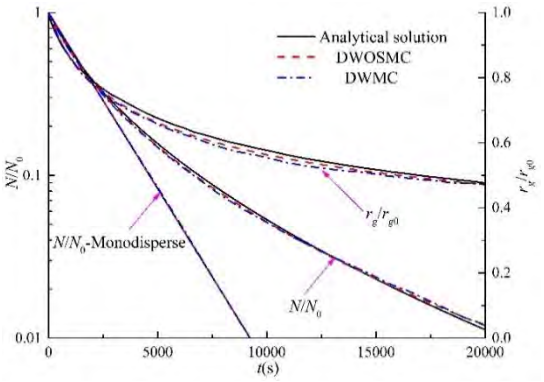

Fig. 2 Variation of N/N_0 and r/r_{g0} for Case A.

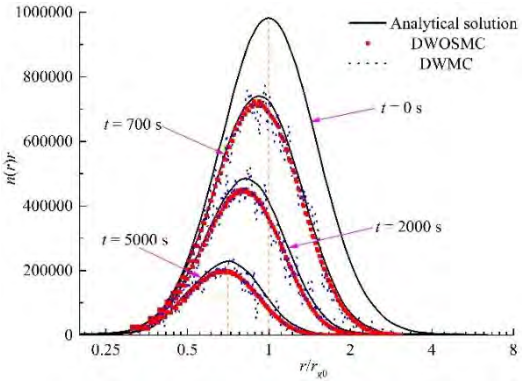

Fig. 3 Variation of PSDs for Case A.

In Case A, a monodispersed particle system is also examined. It can be seen from Fig. 2 that for the gravitational-dominant deposition process, the particle number density reduces as time elapses because of the deposition effect; the particle geometric mean radius also decreases over time since the larger particles have a higher proportion among the deposited particles because of the gravitational effect. For the monodispersed particle system, the results calculated by the DWOSMC and DWMC methods both have perfect agreement with the analytical solutions. In the polydisperse particle system, the results calculated by DWOSMC method and DWMC method are also in accordance with the analytical solutions, and the

calculated particle number density and particle geometric mean radius from DWOSMC are closer to the analytical solutions than the DWMC method.

From Fig. 3, as time elapses, the particle size distribution curves grow narrower and lower because the particle number concentrations at all particle radius become smaller due to the deposition effect. It can also be seen that the peak radius becomes smaller and the curve moves towards the direction of smaller radius, because the larger particles have a higher proportion among the deposited particles due to the gravitational effect, leaving relatively small size particles in the chamber. It can also be seen that the results calculated by the DWOSMC and DWMC methods accord well with analytical solutions, while DWOSMC exhibits much smaller fluctuations than the DWMC method, which shows the improvement in accuracy when predicting the particle size distributions.

In Case B, the deposition process in intermediate size range is considered as is shown in Table 1. Under this condition, the gravitational deposition effect and the Brownian diffusion deposition effect both affect the particle size distribution evolution and neither should be neglected.

The variation of the normalized particle number density and normalized particle geometric mean radius for Case B is shown in Fig. 4, and the evolution of PSDs for several time periods (t = 0 s, 50000 s, 10000 s, 230000 s) is shown in Fig. 5. From Fig. 4, the particle number density reduces as time elapses because of the deposition effect as is expected. The particle geometric mean radius increases over time which is different from Case A, this is because although the larger particles have a higher proportion among the deposited particles due to the gravitational effect, the smaller particles have a higher proportion among

the deposited particles due to the Brownian diffusion effect. Therefore, the variation of the particle geometric mean radius is attributable to the combined effect of the gravitational and Brownian diffusion deposition process. And it can also be concluded that the Brownian diffusion effect dominate the particle size distribution evolution in Case B. From Fig. 5, it can be seen that the particle size distribution curve grows narrower and lower due to the deposition effect. It can also be seen that the peak radius becomes larger and the curve moves in the direction of larger radius, because the Brownian diffusion effect dominate the total deposition process. It can also be seen that the results calculated by the DWOSMC and DWMC methods are in accordance with the analytical solutions, while the DWMC method shows much more fluctuations which is the same with Case A.

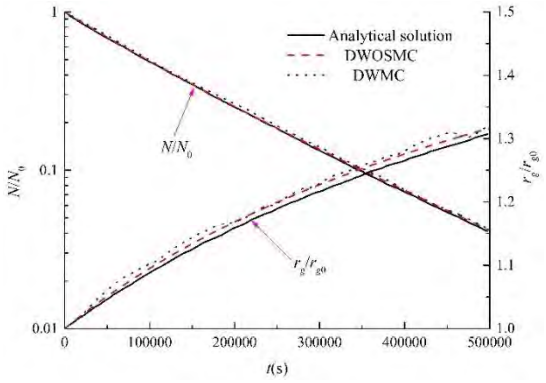

Fig. 4 Variation of N/N_0 and r/r_{g0} for Case B.

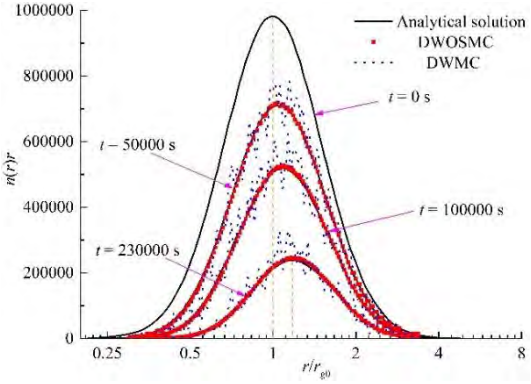

Fig. 5 Variation of PSDs for Case B.

3.2 Case C: wet removal of aerosol particles by precipitation

In case C, the variation of particle size distributions of aerosol particle precipitation by raindrops is investigated. Both the aerosol particles and raindrops are represented by numerical particles with their corresponding “weight”. The Brownian diffusion wet removal mechanism is considered. The scavenging coefficient R_i of simulated particle i is calculated by Eq. (31) [1].

$$R_i(d_a,t)=\int_{d_{r,\min}}^{d_{r,\max}} C_k(d_a,d_r)C_e(d_a,d_r)\mathrm{d}d_r \tag{31}$$

where the collection kernel $C_k(d_a, d_r)$ between aerosol particle a and raindrop r is calculated as Eq. (32), and the collection efficiency $C_e(d_a, d_r)$ is expressed as Eq. (33) [48] .

$$C_k(d_a,d_r)=\pi d_r^{\,2}u(d_r)n_r(d_r)/4 \tag{32}$$

$$C_e(d_a,d_r)=0.7\left[\frac{4}{\sqrt{3}}\left(\frac{1-\alpha}{J+\sigma K}\right)^{1/2}Pe^{-1/2}+2\left(\frac{\sqrt{3}\pi}{4Pe}\right)^{2/3}\left(\frac{(1-\alpha)(3\sigma+4)}{J+\sigma K}\right)^{1/3}\right] \tag{33}$$

where $u(d_r)$ is the falling velocity of the raindrops with diameter of d_r, and α is the volume fraction of the raindrop, $Pe = 3\pi\mu_a d_r u_r d_a^2/(3.328 k_b T\lambda)$, is the Peclet number, $\sigma = \mu_w/\mu_a$, $J = 1\text{-}6\alpha^{1/2}/5+\alpha^2/5$, $K = 1\text{-}9\alpha^{1/3}/5+\alpha+\alpha^2/5$.

In Case C, the initial aerosol particles and raindrops both have lognormal distributions according to Eq. (34).

$$n(d,0)=\frac{1}{d}\frac{N_0}{\sqrt{2\pi}\ln\sigma_0}\exp\left(-\frac{\ln^2(d/d_{g0})}{2\ln^2\sigma_0}\right) \tag{34}$$

The numerical settings and initial conditions of Case C are detailed in Table 2.

Table 2 Initial conditions and numerical settings for Case C.

Particles	N_0 (m^{-3})	d_{g0} (μm)	σ_0	t_{stop} (s)
Aerosols	1×10^6	0.001	1.5	10000
Raindrops	1×10^5	100	1.2	

The variation of normalized particle number density is shown in Fig. 6, and the variation of PSDs for

several time periods (t = 0 s, 600 s, 1200 s, 2400 s, 5400 s, 10000 s) is given in Fig. 7. Fig. 6 indicates that the particle number density decreases over time because of the precipitation process. From Fig. 7, the particle size distribution curves grow narrower and lower and the peak volume of the curve moves gradually towards the direction of larger diameter. The results calculated by the DWOSMC and DWMC methods both have good accordance with the analytical solutions [44].

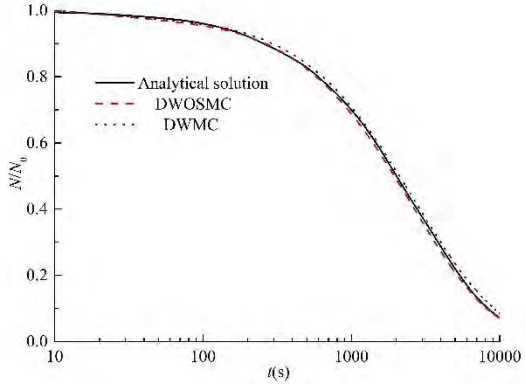

Fig. 6 Variation of N/N_0 for Case C.

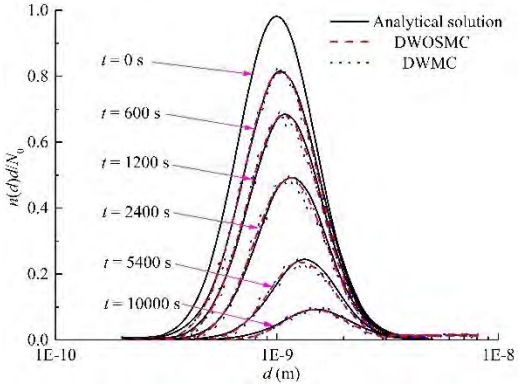

Fig. 7 Variation of PSDs for Case C.

3.3 Case D and Case E: deposition and coagulation processes

In Cases D and E, the initial particles have an exponential size distribution according to Eq. (35).

$$n_{\mathrm{p}}(v,0)=(N_0 / v_{\mathrm{g0}})\,\mathrm{e}^{-v/v_{\mathrm{g0}}} \tag{35}$$

where N_0 and v_{g0} are the initial number density and geometric mean volume of the particles, respectively.

The numerical settings and initial conditions of Cases D and E are detailed in Table 3.

Table 3 Initial conditions and numerical settings for Cases D and E.

Cases	N_0 (cm^{-3})	v_{g0} ($\mu\mathrm{m}^3$)	β ($\mathrm{cm}^3\cdot\mathrm{s}^{-1}$)	R (s^{-1})	t_{stop} (s)
D	1×10^{6}	0.027	6.405×10^{-10}	3.2025×10^{-4}	1560

E	1×10^{6}	0.027	6.405×10^{-10}	$3.3928\times10^{-3}\times v^{2/3}$	1560

In Case D, the coagulation and deposition kernels are both constant as shown in Table 3. The variation of normalized particle number density and normalized geometric mean volume are shown in Fig. 8, and the variation of PSDs (t = 0 s, 750 s, 1500 s) is given in Fig. 9.

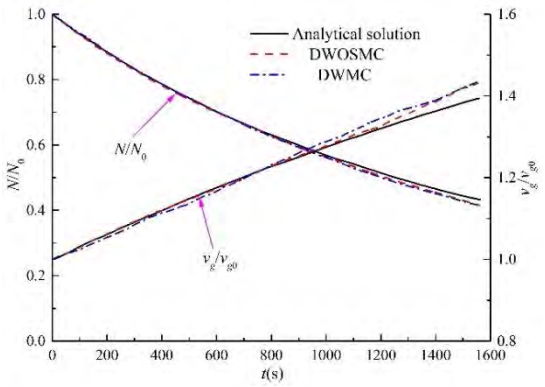

Fig. 8 Variation of N/N_0 and v/v_{g0} for Case D.

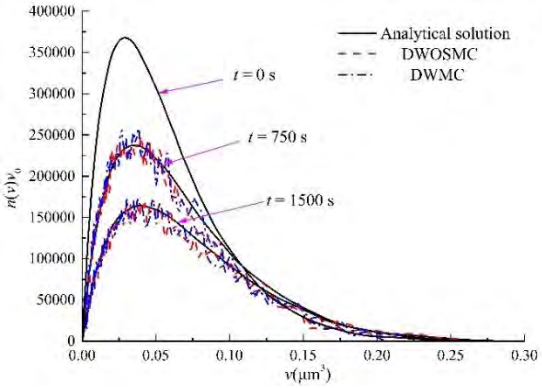

Fig. 9 Variation of PSDs for Case D.

From Fig. 8, as time elapses, the particle number density decreases since both the coagulation process and deposition process will reduce the particle number. The particle geometric mean volume increases due to the coagulation and deposition processes. From Fig. 9, the particle size distribution curves grow narrower and lower due to the coagulation and deposition processes. It can also be seen that the peak volume of the curve almost maintains at the same position which is the combined effect of coagulation and deposition. The PSDs calculated by the DWOSMC and DWMC methods both have good accordance with the analytical solutions [45], and the results calculated by DWOSMC are closer to analytical solutions than the DWMC method when predicting the variation of particle number density and geometric mean volume. For predicting the particle size distributions, it can be seen that the DWOSMC also experience somewhat

fluctuations as the same with the DWOMC method because it also uses stochastic method when dealing with the coagulation process.

For Case E, a coagulation kernel with constant value is adopted and the deposition kernel in gravitational-dominant size range is adopted as shown in Table 3. The variation of normalized particle number density and geometric mean volume are shown in Fig. 10, and the variation of particle size distributions (t = 0 s, 750 s, 1500 s) is shown in Fig. 11.

From Fig. 10, as time elapses, the particle number concentration decreases as is the same with Case D. The particle geometric mean volume does not vary monotonically which is different from Case D. It can be seen that the particle geometric mean volume firstly increases and then decreases over time, which is the combined effect of the coagulation process and deposition process. The coagulation events will make the particle size larger while the gravitational-dominant deposition event will make the particle size smaller. Therefore, it can be concluded that the coagulation dynamics firstly mainly governs the particle dynamical process and then the deposition process dominates the particle dynamical process at the second simulation period. From Fig. 11, the evolution of the particle size distributions shares the same tendency with Case D. The results calculated by the DWOSMC and DWMC methods both have good consistency with the analytical solutions [45].

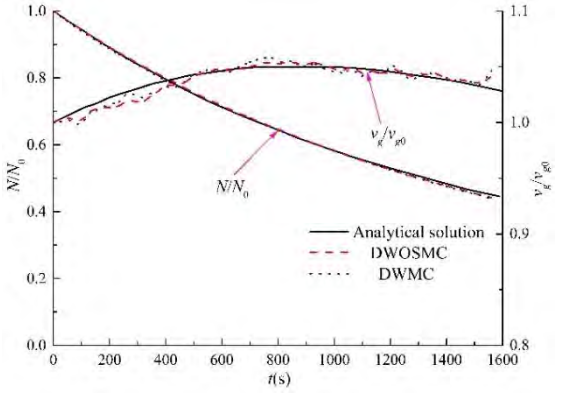

Fig. 10 Variation of N/N_0 and v/v_{g0} for Case E.

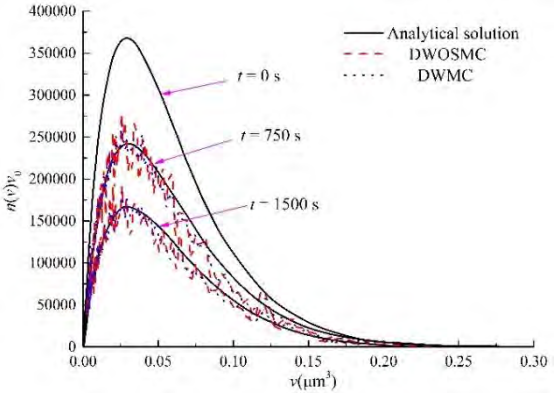

Fig. 11 Variation of PSDs for Case E.

3.4 **Case F: polydisperse sodium chloride aerosol dynamics**

In Case F, the variation of polydisperse sodium chloride aerosols in a closed chamber is observed, the results obtained from DWOSMC are validated against the experimental results provided by Kim et al. [46]. The case where the fan rotation speed is 0 rpm indicates that no turbulence effect should be considered. Particles are initially log-normally distributed with diameter ranging from 30 to 100 nm where Brownian coagulation kernel [49] which is shown in Eq. (7) and constant deposition kernel are considered. The initial conditions and numerical settings are detailed in Table 4.

Table 4 Initial conditions and numerical settings for Case F.

Case	N_0 (m^{-3})	d_{g0} (nm)	σ_0	β ($m^3 \cdot s^{-1}$)	R (s^{-1})	t_{stop} (s)
F	1×10^{12}	50	1.6	Eq. (7)	2.4×10^{-5}	2000

The variations of normalized particle number density and geometric mean diameter are shown in Fig. 12, and the variation of particle size distributions (t = 0 s, 1000 s, 2000 s) is shown in Fig. 13. It can be seen that under this experimental condition, the particle number density decreases over time and the particle diameter increases over time where the coagulation process is dominant. The calculated results from

DWOSMC have good consistency with the experimental results with the maximum relative error of 1.7% and 4% for the particle number density and geometric particle mean diameter, respectively. From Fig. 13, the PSD curves become lower and narrower rapidly over time due to the coagulation and deposition effects, and the peak value of the PSD moves in the direction of larger diameters. The calculated PSD from DWOSMC is consistent with the results from the method of moment (MOM) [50].

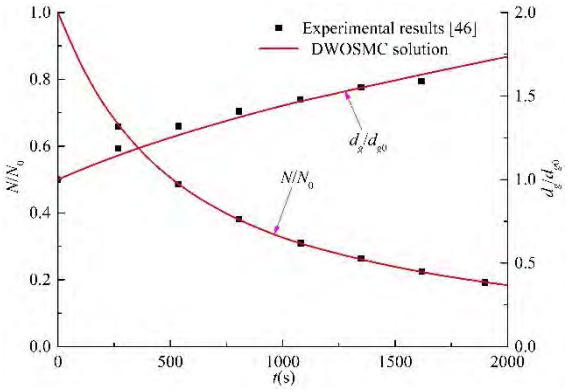

Fig. 12 Variation of N/N_0 and d/d_{g0} for Case F.

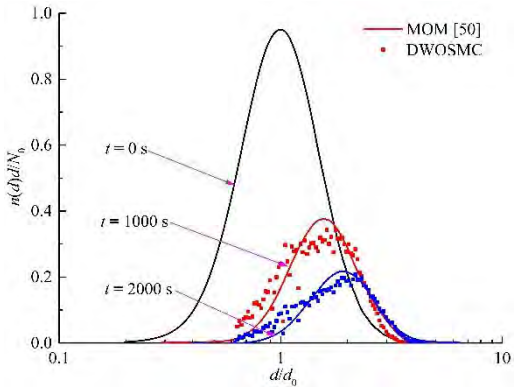

Fig. 13 Variation of PSDs for Case F.

3.5 Case G: paper ash particle deposition and coagulation dynamics

In case G, the variation of PSDs of polydisperse paper ash particles in an enclosed chamber is investigated, the calculated results from DWOSMC are validated against the experimental results provided by Schnell et al. [47]. The particles are initially log-normally distributed where constant coagulation and deposition kernels are considered. The initial conditions and numerical settings are detailed in Table 5.

Table 5 Initial conditions and numerical settings for Case G.

Case	N_0 (m^{-3})	d_{g0} (μm)	σ_0	β ($m^3 \cdot s^{-1}$)	R (s^{-1})	t_{stop} (s)
G	1.36×10^{12}	0.079	1.57	1.22×10^{-15}	2.68×10^{-4}	3600

The evolution of particle geometric mean diameter for Case G is shown in Fig. 14. The particle

geometric mean diameter after 2100s provided by Schnell et al. [47] is 0.133 μm, and the calculated result by DWOSMC method is 0.135 μm, the relative error is 1.5% which is quite small, so it can be concluded that the numerically calculated results obtain quite high consistency with the experimental results for paper ash particles in an enclosed chamber considering constant coagulation and deposition processes.

The variation of particle size distributions (t = 0 s, 600 s, 2100 s) for Case G is shown in Fig. 15. It can be seen that in this experimental condition, the particle size distribution curves become lower and narrower over time due to the coagulation and deposition effects, and the peak value of the PSD moves gradually in the direction of larger diameters. The results calculated by the DWOSMC method accord well with the experimental results expect for some fluctuations.

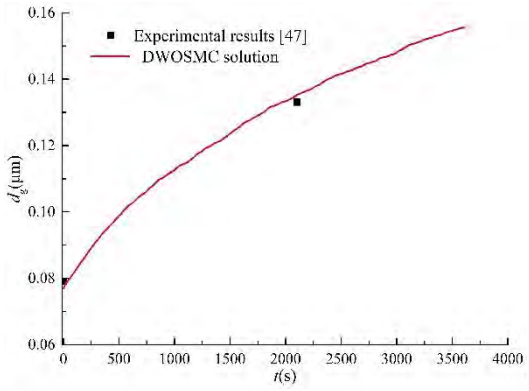

Fig. 14 Variation of particle geometric diameter for Case G.

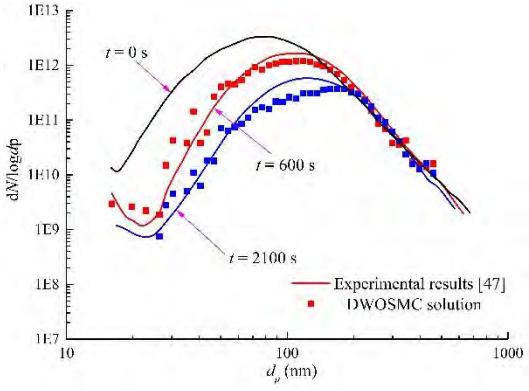

Fig. 15 Variation of PSDs for Case G.

3.6 Case H: nanoparticle deposition and coagulation dynamics in a vacuum chamber

In case H, the evolution of nanoparticles in a vacuum chamber is investigated. The particles are initially uniformly distributed with a diameter of 5 nm where coagulation kernel in free molecular regime and deposition kernel in diffusion-dominant range are considered. The results from vacuum condition

(p=0.5 atm) are compared with that from standard atmospheric condition. The calculated results from the DWOSMC method is compared with a sectional method (SM) [25] for the purpose of validation and comparison. The initial conditions and numerical settings are detailed in Table 6.

Table 6 Initial conditions and numerical settings for Case H.

Cases	N_0 (m^{-3})	d_0 (nm)	β ($m^3 \cdot s^{-1}$)	R (s^{-1})	t_{stop} (s)
H	1×10^{14}	5	Eq. (7)	Eq.(28)	4000

The variations of normalized particle number density and total particle volume are shown in Fig. 16, and the variation of particle size distributions (t = 1000 s, 2000 s) is shown in Fig. 17.

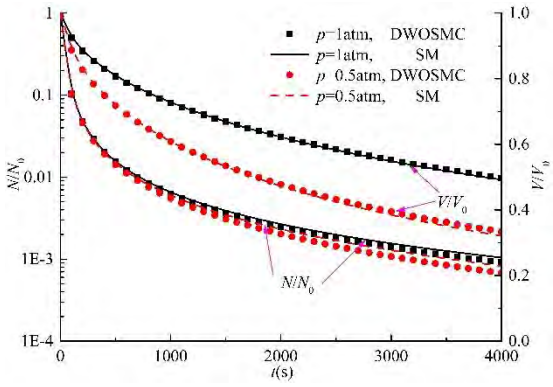

Fig. 16 Variation of N/N_0 and V/V_0 for Case H.

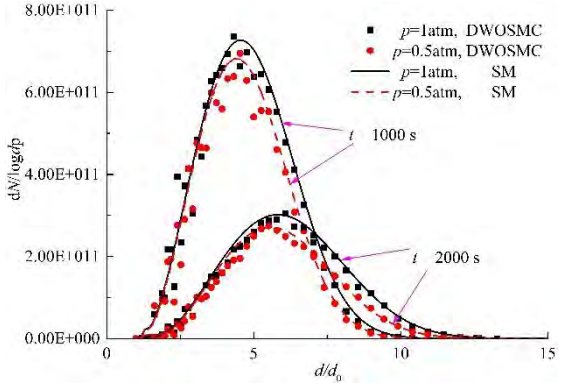

Fig. 17 Variation of PSDs for Case H.

It can be seen that the particle number density under vacuum condition is slightly smaller than that in atmospheric condition, and the total particle volume under vacuum condition is much smaller than that in atmospheric condition, which indicates that the deposition rate is larger under vacuum condition than that in atmospheric condition. The particle size distribution curves obtained from vacuum condition are lower and narrower than that from the atmospheric condition. And it can also be seen that the peak diameter becomes slightly smaller in vacuum condition. Since the Brownian diffusion deposition events and the

coagulation events will both make the mean particle diameter larger, and the deposition rate is larger in the vacuum condition, it can be concluded that the coagulation rate is smaller in vacuum condition than that in atmospheric condition under the initial condition of Case H. It can also be seen from Figs. 16 and 17 that the calculated results from DWOSMC method agree well with the sectional method.

3.7 Accuracy and Efficiency Discussion and Assessment

To further assess the simulation precision and efficiency of this further developed DWOSMC model for predicting particle deposition and coagulation processes, the maximum relative error $\varepsilon_{\max}$ and the non-dimensional computational time ζ are used and expressed as Eq. (36) and Eq. (37), respectively.

$$\varepsilon_{\max} = \left| \frac{X(t) - X_a(t)}{X_a(t)} \right|_{\max} \times 100\% \tag{36}$$

$$\zeta = \frac{t_s}{t_A} \tag{37}$$

where $X_a(t)$ is the analytical solution, $X(t)$ is the calculated result from the numerical simulation method (i.e., DWOSMC and DWMC methods), t_A is the simulation time needed for DWOSMC method for Case A, and t_s is the simulation time needed for different cases and methods.

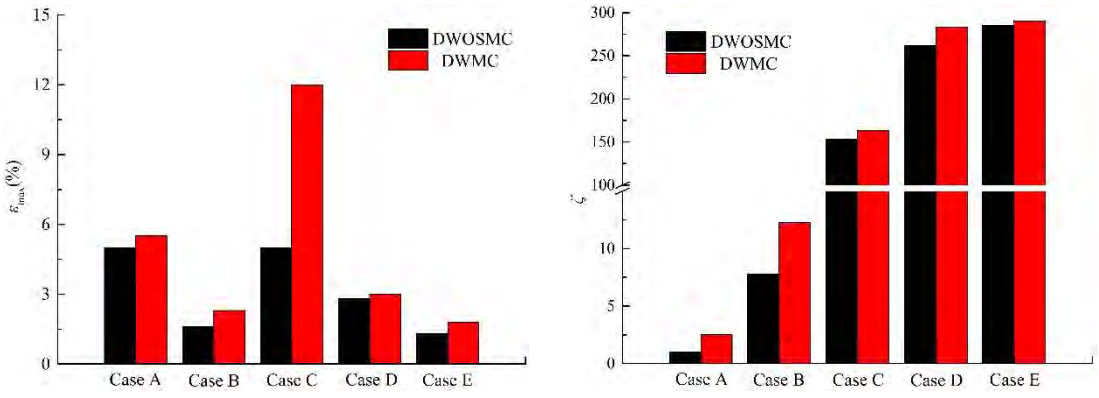

Fig. 18 Comparison of maximum relative error ε_{max} derived from Cases A to E using the DWOSMC and DWMC methods.

Fig. 19 Comparison of normalized computational time ζ from Cases A to E using the DWOSMC and DWMC methods.

The ε_{max} calculated from Cases A to E is shown in Fig. 18 (for Cases A and B, the ε_{max} was calculated from the particle geometric mean radius; for Case C, the ε_{max} was calculated from the particle number density; for Cases D and E, the ε_{max} was calculated from the particle geometric mean volume). The computation time used for different cases is given in Fig. 19. It can be seen that for Cases A to E, the maximum relative error calculated by the DWOSMC method is smaller than the DWMC method and the computation time used for DWOSMC method is also less than the DWMC method, which proves that the further developed DWOSMC method exhibits higher computational accuracy and efficiency than the DWMC method when predicting particle deposition and coagulation processes. Furthermore, from Sections 3.4 and 3.5, when comparing with the experimental results, the relative error based on the particle geometric mean volume or diameter is only 4% and 1.5% when using the DWOSMC method for predicting sodium chloride aerosol dynamics and paper ash particle dynamics, respectively. So it can be concluded that the developed DWOSMC method has quite high accuracy and efficiency for predicting particle dynamics considering coagulation and deposition processes.

4. Conclusions

In this study, the particle size distributions (PSDs) evolution of polydisperse particle systems experiencing deposition and coagulation dynamics in enclosed chambers are investigated. A differentially weighted operator splitting Monte Carlo (DWOSMC) method is further developed for predicting particle

dynamics including deposition and coagulation processes. In this DWOSMC method, the deposition event is solved by a deterministic method where a proportion of the deposited real particles inside a simulated particle is determined by a probability related to the deposition kernel. The calculated results are validated against the analytical solutions and experimental results. The conclusions of the present study are as follows.

(1) In the size range of particles studied herein, particle deposition and coagulation processes would happen spontaneously and the thermodynamics associated with the particle dynamical behaviours are implicitly included in the model formulation of coagulation and deposition kernels, and these two stochastic processes increase the entropy and reduce the Gibbs free energy.

(2) In the first five cases, deposition and coagulation processes or particle precipitation process are examined and the results calculated from DWOSMC method have good accordance with the analytical solutions, and the DWOSMC method exhibits higher accuracy and efficiency than the DWMC method. In the sixth and seventh cases, the results calculated from DWOSMC have good consistency with the experimental data for predicting the particle size distributions of sodium chloride aerosol particles and paper ash particles.

(3) Compared with the case in standard atmospheric condition, the particle deposition rate is larger under vacuum condition.

Therefore, this further developed and fully validated DWOSMC method turns out to be a good candidate for solving particle deposition and coagulation dynamics with satisfactory improvement in both computational accuracy and efficiency.

Acknowledgements

The development of the proposed Monte Carlo method was supported by the financial support from National Natural Science Foundation of China (No. 51806048), China, Key Foundation of Science and Technology on Combustion, Internal Flow and Thermal-Structure Laboratory (6142701190106), Xi'an, China and the Program of Shenzhen Technology Projects (JCYJ20180306171941256), Shenzhen, China. This work was also supported by the grants from the General Research Fund, Research Grants Council of the Hong Kong Special Administrative Region, China (Project No. PolyU 152125/15E), and the Central Research Grant of The Hong Kong Polytechnic University (Project No. B-Q47Y), Hong Kong. Lastly, the present work is the further development and extension of the developed differentially weighted operator splitting Monte Carlo (DWOSMC) method during the first author's PhD study at the Department of Mechanical Engineering in The Hong Kong Polytechnic University.

References

[1] H. Zhao, C. Zheng, Monte Carlo solution of wet removal of aerosols by precipitation, Atmos. Environ. 40 (2006) 1510–1525.

[2] R. Weber, N. Schaffel-Mancini, M. Mancini, T. Kupka, Fly ash deposition modelling: Requirements for accurate predictions of particle impaction on tubes using RANS-based computational fluid dynamics, Fuel. 108 (2013) 586–596.

[3] M. Ketzel, R. Berkowicz, Modelling the fate of ultrafine particles from exhaust pipe to rural background: An analysis of time scales for dilution, coagulation and deposition, Atmos. Environ. 38 (2004) 2639–2652.

[4] C. Wang, H.K. Sung, N.Y. Kim, Aerosol deposition-based micropatterning of barium titanate via sulphur hexafluoride inductively coupled plasma etching, Vacuum. 114 (2015) 49–53.

[5] R. Panickar, C.B. Sobhan, S. Chakravorti, Chemical vapor deposition synthesis of carbon spheres: Effects of temperature and hydrogen, Vacuum. 172 (2020) 1–10.

[6] C.B. Almquist, P. Biswas, Role of synthesis method and particle size of nanostructured TiO2 on its photoactivity, J. Catal. 212 (2002) 145–156.

[7] P. Verma, M. Jafari, S.M.A. Rahman, E. Pickering, S. Stevanovic, A. Dowell, R. Brown, Z. Ristovski, The impact of chemical composition of oxygenated fuels on morphology and nanostructure of soot particles, Fuel. 259 (2020) 1–11.

[8] Y. Wang, L. Chen, R. Chen, G. Tian, D. Li, C. Chen, X. Ge, G. Ge, Effect of relative humidity on the deposition and coagulation of aerosolized SiO2 nanoparticles, Atmos. Res. 194 (2017) 100–108.

[9] N.T.K. Thanh, N. Maclean, S. Mahiddine, Mechanisms of nucleation and growth of nanoparticles in solution, Chem. Rev. 114 (2014) 7610–7630.

[10] S.H. Lee, H. Gordon, H. Yu, K. Lehtipalo, R. Haley, Y. Li, R. Zhang, New particle formation in the atmosphere: from molecular clusters to global climate, J. Geophys. Res. Atmos. 124 (2019) 7098–7146.

[11] H. Wang, Formation of nascent soot and other condensed-phase materials in flames, Proc. Combust. Inst. 33 (2011) 41–67.

[12] V. Šíp, L. Beneš, Dry deposition model for a microscale aerosol dispersion solver based on the moment method, J. Aerosol Sci. 107 (2017) 107–122.

[13] L. Pichelstorfer, R. Winkler-Heil, W. Hofmann, Lagrangian/Eulerian model of coagulation and deposition of inhaled particles in the human lung, J. Aerosol Sci. 64 (2013) 125–142.

[14] K. Okuyama, Y. Kousaka, M. Adachi, Coagulation and deposition of aerosol partilces in a flow type chamber, J. Aerosol Sci. 11 (1980) 11–22.

[15] T. Hussein, A. Hruška, P. Dohányosová, L. Džumbová, J. Hemerka, M. Kulmala, J. Smolík, Deposition rates on smooth surfaces and coagulation of aerosol particles inside a test chamber, Atmos. Environ. 43 (2009) 905–914.

[16] D. Rim, M. Green, L. Wallace, A. Persily, J. Il Choi, Evolution of ultrafine particle size distributions following indoor episodic releases: Relative importance of coagulation, deposition and ventilation, Aerosol Sci. Technol. 46 (2012) 494–503.

[17] M. Yu, A.J. Koivisto, K. Hämeri, M. Seipenbusch, Size Dependence of the Ratio of Aerosol Coagulation to Deposition Rates for Indoor Aerosols, Aerosol Sci. Technol. 47 (2013) 427–434.

[18] Y. Xiao, Y. Lv, Y. Zhou, H. Liu, J. Liu, Size-resolved surface deposition and coagulation of indoor particles, Int. J. Environ. Health Res. 30 (2020) 251–267.

[19] S. Friedlander, Smoke, dust and haze. Fundamentals of aerosol behaviour., Oxford University Press, New York, 1977.

[20] T.L. Chan, S.Y. Liu, H.J. Liu, A numerical study on particle formation and evolution of a vehicular

exhaust plume using the bimodal TEMOM, Particuology. 43 (2019) 46–55.

[21] M. Yu, J. Lin, J. Cao, M. Seipenbusch, An analytical solution for the population balance equation using a moment method, Particuology. 18 (2015) 194–200.

[22] R. McGraw, Description of aerosol dynamics by the quadrature method of moments, Aerosol Sci. Technol. 27 (1997) 255–265.

[23] K.W. Lee, H. Chen, J.A. Gieseke, Log-Normally preserving size distribution for brownian coagulation in the free-molecule regime, Aerosol Sci. Technol. 3 (1984) 53–62.

[24] M. Yu, J. Lin, T. Chan, A new moment method for solving the coagulation equation for particles in Brownian motion, Aerosol Sci. Technol. 42 (2008) 705–713.

[25] A. Prakash, A.P. Bapat, M.R. Zachariah, A Simple Numerical Algorithm and Software for Solution of Nucleation, Surface Growth, and Coagulation Problems, Aerosol Sci. Technol. 37 (2003) 892–898.

[26] Z. Chen, F. Yuan, R.J. Jiang, Different approximate models of the sectional method for nanoparticle Brownian coagulation, Int. J. Numer. Methods Heat Fluid Flow. 25 (2015) 438–448.

[27] H. Liu, T.L. Chan, A coupled LES-Monte Carlo method for simulating aerosol dynamics in a turbulent planar jet, Int. J. Numer. Methods Heat Fluid Flow. 30 (2019) 855–881.

[28] H.M. Liu, T.L. Chan, Two-component aerosol dynamic simulation using differentially weighted operator splitting Monte Carlo method, Appl. Math. Model. 62 (2018) 237–253.

[29] G. Kotalczyk, F.E. Kruis, A Monte Carlo method for the simulation of coagulation and nucleation

based on weighted particles and the concepts of stochastic resolution and merging, J. Comput. Phys. 340 (2017) 276–296.

[30] C. Mitsakou, C. Helmis, C. Housiadas, Eulerian modelling of lung deposition with sectional representation of aerosol dynamics, J. Aerosol Sci. 36 (2005) 75–94.

[31] K. Zhou, X. Jiang, T.L. Chan, Error analysis in stochastic solutions of population balance equations, Appl. Math. Model. 80 (2020) 531–552.

[32] H. Zhao, F.E. Kruis, C. Zheng, Reducing statistical noise and extending the size spectrum by applying weighted simulation particles in monte carlo simulation of coagulation, Aerosol Sci. Technol. 43 (2009) 781–793.

[33] R.E.L. DeVille, N. Riemer, M. West, Weighted Flow Algorithms (WFA) for stochastic particle coagulation, J. Comput. Phys. 230 (2011) 8427–8451.

[34] H. Liu, T.L. Chan, Differentially weighted operator splitting Monte Carlo method for simulating complex aerosol dynamic processes, Particuology. 36 (2018) 114–126.

[35] H. Zhao, F.E. Kruis, C. Zheng, A differentially weighted Monte Carlo method for two-component coagulation, J. Comput. Phys. 229 (2010) 6931–6945.

[36] H. Zhao, C. Zheng, A new event-driven constant-volume method for solution of the time evolution of particle size distribution, J. Comput. Phys. 228 (2009) 1412–1428.

[37] H. Vehkamäki, I. Riipinen, Thermodynamics and kinetics of atmospheric aerosol particle formation and growth, Chem. Soc. Rev. 41 (2012) 5160–5173.

[38] N. Kourti, A. Schatz, Solution of the general dynamic equation (GDE) for multicomponent aerosols, J. Aerosol Sci. 29 (1998) 41–55.

[39] H. Liu, Monte Carlo simulation of aerosol dynamics in turbulent flows, The Hong Kong Polytechnic University, 2019.

[40] Z. Xu, H. Zhao, C. Zheng, Fast Monte Carlo simulation for particle coagulation in population balance, J. Aerosol Sci. 74 (2014) 11–25.

[41] K. Liffman, A direct simulation Monte-Carlo method for cluster coagulation, J. Comput. Phys. 100 (1992) 116–127.

[42] R.I. McLachlan, G.R.W. Quispel, Splitting methods, Acta Numer. 2002. (2010) 341–434.

[43] S.H. Park, K.W. Lee, Analytical solution to change in size distribution of polydisperse particles in closed chamber due to diffusion and sedimentation, Atmos. Environ. 36 (2002) 5459–5467.

[44] C.H. Jung, Y.P. Kim, K.W. Lee, Analytic solution for polydispersed aerosol dynamics by a wet removal process, J. Aerosol Sci. 33 (2002) 753–767.

[45] M.M.R. Williams, Some exact and approximate solutions of the nonlinear Boltzmann equation with applications to aerosol coagulation, J. Phys. A. Math. Gen. 14 (1981) 2073–2089.

[46] D.S. Kim, S.B. Hong, Y.J. Kim, K.W. Lee, Deposition and coagulation of polydisperse nanoparticles by Brownian motion and turbulence, J. Aerosol Sci. 37 (2006) 1781–1787.

[47] M. Schnell, C.S. Cheung, C.W. Leung, Investigation on the coagulation and deposition of combustion particles in an enclosed chamber with and without stirring, J. Aerosol Sci. 37 (2006)

1581–1595.

[48] C.H. Jung, K.W. Lee, Filtration of Fine Particles by Multiple Liquid Droplet and Gas Bubble Systems, Aerosol Sci. Technol. 29 (1998) 389–401.

[49] S.E. Pratsinis, Simultaneous nucleation, condensation, and coagulation in aerosol reactors, J. Colloid Interface Sci. 124 (1988) 416–427.

[50] G. Xu, J. Wang, Development and application of moment method on nanoparticles evolution due to coagulation and deposition, J. Hydrodyn. 31 (2019) 1011–1020.

Figure Caption:

Table Caption: